Towards Accurate Pixel-wise Object Tracking by Attention Retrieval

Zhipeng Zhang[1] Bing Li[1] Weiming Hu[1] Houwen Peng[2]
[1] NLPR, CASIA & UCAS [2]Microsoft Research
zhangzhipeng2017@ia.ac.cn houwen.peng@microsoft.com

Abstract

The encoding of the target in object tracking moves from the coarse bounding-box to fine-grained segmentation map recently [21]. Revisiting de facto real-time approaches that are capable of predicting mask during tracking, we observed that they usually fork a light branch from the backbone network for segmentation [39, 26]. Although efficient, directly fusing backbone features without considering the negative influence of background clutter tends to introduce false-negative predictions, lagging the segmentation accuracy. To mitigate this problem, we propose an attention retrieval network (ARN) to perform soft spatial constraints on backbone features. We first build a look-up-table (LUT) with the ground-truth mask in the starting frame, and then retrieves the LUT to obtain an attention map for spatial constraints. Moreover, we introduce a multi-resolution multi-stage segmentation network (MMS) to further weaken the influence of background clutter by reusing the predicted mask to filter backbone features. Our approach set a new state-of-the-art on recent pixel-wise object tracking benchmark VOT2020 while running at 40 fps. Notably, the proposed model surpasses SiamMask [39] by 11.7/4.2/5.5 points on VOT2020, DAVIS2016, and DAVIS2017, respectively. We will release our code at https://github.com/researchmm/TracKit.

1. Introduction

Visual object tracking (VOT), which aims at estimating the target's location and scale in each frame of a video sequence, is one of the most fundamental yet challenging tasks in the computer vision field. Recently, the tracking community starts focusing on replacing the classical rectangle box with a segmentation mask to encode the target. The benchmark with new evaluation methodology, *i.e.,* VOT2020 [21] has been introduced, which requires the algorithm to robustly track the target while predicting an accurate binary mask. The task of video object segmentation (VOS) is akin to object tracking, yet it typically considers large targets observed for less than 100 frames with low background distractor presence. Top-ranked VOS approaches thus fare poorly in challenging tracking scenarios, as shown in Fig. 1.

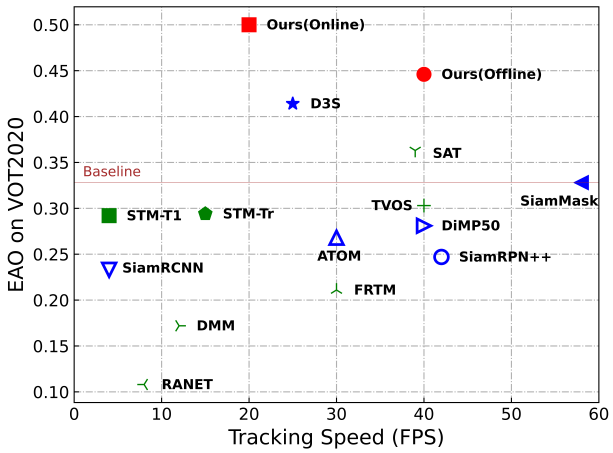

Figure 1. Expected Average Overlap (EAO) versus running speeds (frame-per-second) on the recent pixel-wise tracking benchmark [21]. We evaluate the state-of-the-art VOT (blue) and VOS methods (green). The hollow blue markers denote VOT methods predicting a bounding box instead of a segmentation mask. It shows that the top-ranked VOS methods perform unsatisfactorily on the new pixel-wise tracking benchmark.

To simultaneously deal with tracking and segmentation, several state-of-the-art approaches have been proposed. One mainstream is using an off-the-shelf image segmentation network, *e.g.,* MaskRCNN [15], Box2Seg [6] to predict a binary mask inside the bounding box given by the tracking model [37]. However, due to the error accumulation in tracking, the predicted bounding box may become unreliable. As a consequence, the segmentation of target objects will be misled. Moreover, this paradigm is hard to run in real-time speeds, since the well-performed image segmentation network generally requires massive computation. Alternatively, SiamMask [39] and D3S [26] fork delicately designed segmentation side branch to predict target mask, introducing small computational overheads. They progressively upscale features from different depths of backbone

networks into a detailed segmentation map. Nevertheless, background clutter in raw backbone features tends to introduce false-positive predictions in segmentation because of its similar semantics with the target objects. Weakening the negative influence of background clutter is thus necessary in order to improve segmentation accuracy.

In this paper, we set out to reduce the false-positive predictions in the paradigm of tracking with a segmentation side branch like SiamMask [39] and D3S [26], while keeping its efficiency, *i.e. run in real-time speeds*. To achieve the goal, we propose a novel attention retrieval network (ARN) to set up soft spatial constraints on features for segmentation. Specifically, we first build a look-up-table (LUT) to store feature and binary mask of the starting frame. The embedding of each spatial location in the feature is considered as an *address*, while its corresponding mask (0 or 1) is the *value* of the LUT. The ARN then retrieve the LUT to generate an attention map by learning an affinity matrix based on the similarities between feature of frame T (F_t) and *addresses* in the LUT. By adding the attention map to the features F_t, we can suppress the negative influence induced by clutter in the background. Moreover, we introduce a multi-resolution multi-stages segmentation network (MMS) after ARN to further weaken the background clutter by reusing the predicted mask to filter backbone features.

The attention retrieval network requires a mask in the starting frame. To handle videos with only a bounding box at the beginning of tracking, we propose a cyclic initialization strategy. Concretely, we first generate a pseudo mask with the ground-truth box to initialize the LUT. After that, we pass the starting frame through the model and predict a mask. The predicted mask is then used to re-initialize the LUT. We cyclically perform the re-initialization several times, achieving an accurate mask for the starting frame. The cyclic initialization improves the adaption of our work.

We build a new tracking and segmentation framework based on the ARN and MMS. Experiments show that the proposed model achieves EAO of 0.444 on VOT2020, outperforming SiamMask (0.328) and D3S (0.414) while running at $40fps$. Moreover, our work also surpasses SiamMask and D3S on all seven criteria of DAVIS2017.

The main contributions of this work are as follows.

- We propose a novel attention retrieval network to perform soft spatial constraints on features for segmentation. Equipped with the multi-resolution multi-stage segmentation network, the negative influence induced by the background clutter is effectively suppressed.

- We introduce a cyclic initialization strategy to handle videos without mask in the starting frame. The proposed strategy guarantees the adaption of our model on videos with bounding box or mask initialization.

- We build a tracking and segmentation pipeline based on the proposed ARN and MMS. Experimental results demonstrate that our model set a new state-of-the-art performance on the recent introduced tracking benchmark [21] while running in per-frame real-time speeds.

2. Related Work

In this section, we review the video object tracking and segmentation approaches, as well as briefly review the attention mechanisms in computer vision.

2.1. Video Object Tracking

Video object tracking is formulated as a sequential bounding box estimation problem. Given the target and its state in the first frame, one algorithm is required to predict the target's bounding boxes in the subsequent frames. The community has proposed massive approaches to tackle challenges in realistic tracking scenarios. To date, object tracking is dominated by correlation-filter (CF) and Siamese paradigms. Correlation-filter based approaches consider tracking as a ridge regression problem and solve it by the circular correlation in the frequency domain [16, 12, 11]. Siamese trackers learn a matching network by offline training on tremendous data [2, 24, 49]. As our approach is performed in the Siamese structure, we review the related methods in this section, and we refer the readers to [28] for more details about correlation-filter (CF) based approaches.

The pioneering work of Siamese trackers, *i.e.*, SiamFC [2], employs a fully-convolutional network to offline train a similarity metric for target matching. Later, SiamRPN [24] improves it by introducing a region proposal network to estimate the target's scale. The follow-up works unleash the capability of deeper backbone networks in Siamese trackers by eliminating matching inconsistency and position bias [49, 23]. Recently, the anchor-free mechanism becomes popular due to its simple design and leading performance [50, 45]. One distinct trend in object tracking is to predict a binary mask for the tracked target. The VOT2020 benchmark replaces the bounding box label to mask and propose a new methodology for tracker evaluation. SiamRCNN [37] considers the predicted bounding box as hard spatial constraints, and uses an existing segmentation model to estimate the mask in the box. Conversely, SiamMask [39] and D3S [26] directly fork a segmentation branch in the original tracking network, running much faster than SiamRCNN [37]. However, without spatial constrains, they often suffer from false-positive predictions. In this work, we mitigate this problem by proposing an attention retrieval network to set soft constraints in the feature map for segmentation.

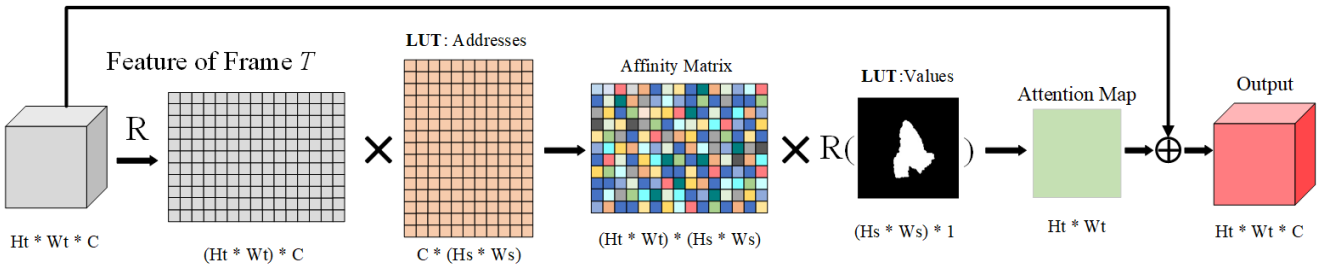

Figure 2. Pipeline of the attention retrieval network (ARN). We first multiply the feature of frame T, *i.e.* F_t, to *addresses* in LUT, attaining an affinity matrix. Then the attention map is produced by the multiplication between the affinity matrix and *values* in LUT. Finally, we add the attention map to F_t to set soft spatial constraints.

2.2. Video Object Segmentation

The focused task in this paper is closely related to the semi-supervised video object segmentation (VOS). We thus review the frameworks in VOS first, and then compare the differences between VOT and VOS. Semi-supervised VOS algorithms concentrate on predicting an accurate mask representation of the target given mask in the starting frame. The segmentation-by-detection paradigm [5, 27] first predicts the bounding box of the target and then classify each pixel in the box to the foreground or background. It treats targets in different frames independently. The aforementioned tracking method SiamRCNN [37] belongs to this stream. On the contrary, the propagation-based paradigm [29, 48, 18, 30, 35] learns an object mask propagator to exploit consistency between video frames. It improves the mask smoothness in adjacent frames. The proposed attention retrieval network is inspired by the recent propagation-based model [48], which propagates the predicted masks based on feature similarities. In our work, instead of directly propagating masks, we generate a soft constraint map based on feature affinity matrix, and use it to guide the learning of the segmentation network.

VOS and VOT are conceptually similar, especially when the recent tracking benchmark requires the algorithms to predict binary mask instead of rectangle box. We argue that the main difference between VOT and VOS lies in the data distribution. VOS task typically considers large targets observed for less than 100 frames with low background distractor presence, while videos in VOT are usually more challenging. We discuss the details of the comparison between VOS and VOT in Sec. 5.

2.3. Attention Mechanism

Attention plays an important role in human perception [19]. Several attempts have been proposed to incorporate attention processing to improve the performance of CNNs in classification [17], detection [13], tracking [38] and segmentation [14]. SENet [17] introduces a compact Squeeze-and-Excitation module to exploit the inter-channel relationship. Domain attention introduced in [40] consists of a bank of the SE adapters, enabling substantially better multi-domain detection. RASNet [38] combines spatial and channel attention to refine feature maps. In most existing attention modules, the attention map is generated from the feature itself. The interpretability is weak since the transition mechanism from feature space to attention space is unknown. In contrast, our attention retrieval network has a fixed look-up-table (LUT), containing the *values* (0 or 1) and *addresses* (embeddings) for retrieving to generate an attention map. The attention map is utilized as soft spatial constraints to weaken the influence of background clutter and distractors. The retrieval mechanism based on feature similarities makes our framework more interpretable.

3. Method

The proposed framework is designed to tackle challenging pixel-wise tracking seniors. It consists of three main steps, *i.e, tracking-retrieval-segmentation*. We follow the recent approach [50] to perform object tracking and will describe it in Sec. 4. In this section, we first detail the attention retrieval network (ARN), in Sec. 3.1, followed by the introduced multi-resolution multi-stage segmentation network (MMS) in Sec. 3.2. For videos without masks in the starting frame, we propose a cyclic initialization strategy to handle this situation, detailed in Sec. 3.3. We finally discuss the differences between our method with other attention mechanisms in Sec. 3.4.

3.1. Attention Retrieval Network

Pixel-wise tracking is challenging since the background clutter can easily induce false-positive predictions. One direct way to mitigate this problem is to set up a hard spatial constraint when segment the target, *e.g.* using bounding boxes. However, the inaccurate box in tracking will mislead the segmentation. We relax the hard constraint to a soft attention map in our retrieval network.

Bulid Look-Up-Table (LUT). We formulate the attention generation as a process of retrieving a LUT. The LUT can be viewed as a memory bank, which stores the reference features (*addresses*) $\mathbf{A} \in \mathbb{R}^{K\times C}$ and the corresponding pixel-wise mask probabilities (*values*) $\mathbf{V} \in \mathbb{R}^{K\times 1}$, where K is the number of *address-value* pairs and C is the channels. There are two ways to build the LUT, *i.e.,* fully-supervised and weakly-supervised. The fully-supervised way only considers the features of the starting frame and its **labeled** mask as *address-value* pairs. The weakly-supervised way also includes the features and the **predicted** masks in the subsequent frames. In our experiments, we observed that the weakly-supervised way does not bring further improvements under VOT settings. We thus simply build the LUT with the starting frame. Concretely, we pass the starting frame through the backbone network followed with a 1×1 convolution layer for channel compression, giving features with the size of $H_s\times W_s\times 64$. The corresponding mask is then downsampled to have the same spatial size, *i.e.,* $H_s\times W_s\times 1$. To the end, the size K of the LUT equals to $H_s\times W_s$ under fully-supervised setting.

Retrieval via Affinity Learning. We aim at predicting an attention map to set up spatial constraints on features for segmentation. The attention map of a feature is generated by retrieving the LUT. Specifically, we first pass the image of frame T through the backbone network followed by a 1×1 convolution layer to get its feature map $\mathbf{F_t} \in \mathbb{R}^{H_t\times W_t\times 64}$. For each embedding $\mathbf{f_i} \in \mathbb{R}^{1\times1\times64}$ in the feature map $\mathbf{F_t}$, we attach it with an attention value determined by its affinity with the *addresses* in the LUT,

$$s_{ij} = \mathbf{f_i} \circ \mathbf{a_j} \tag{1}$$

where $\circ$ indicates dot-product, $\mathbf{a_j} \in \mathbf{A}$ is an *address* in LUT, s_{ij} denotes the affinity between $\mathbf{f_i}$ and $\mathbf{a_j}$. Thus, for each embedding in $\mathbf{F_t}$, its affinity to all *addresses* in LUT are,

$$\mathbf{S} = softmax(\mathcal{R}(\mathbf{F_t}) * \mathcal{R}(\mathbf{A})) \tag{2}$$

where $\mathcal{R}$ is reshape operation. The shape of $\mathcal{R}(\mathbf{F_t})$, $\mathcal{R}(\mathbf{A})$ and $\mathbf{S}$ is $H_tW_t\times 64$, $64\times H_sW_s$, $H_tW_t\times H_sW_s$, respectively. $*$ indicates tensor multiplication. With the affinity matrix $\mathbf{S}$, the attention map is generated by,

$$\mathbf{M} = \mathbf{S} * \mathbf{V} \tag{3}$$

The attention map mesures the probilities of spatial locations in $\mathbf{F_t}$ being the target. We then perform element-wise addition between $\mathbf{M}$ and $\mathbf{F_t}$ to get an enhanced feature $\hat{\mathbf{F}}_\mathbf{t}$. The foreground embeddings will be enhanced due to their larger attention values. The retrieval process is depicited in Fig. 2.

The attention map is indeed soft spatial constraints, which increases the influence of locations at foreground embeddings. Compared to the hard constraints induced by bounding boxes, our approach is more flexible and not affected by the inaccurate bounding box in tracking.

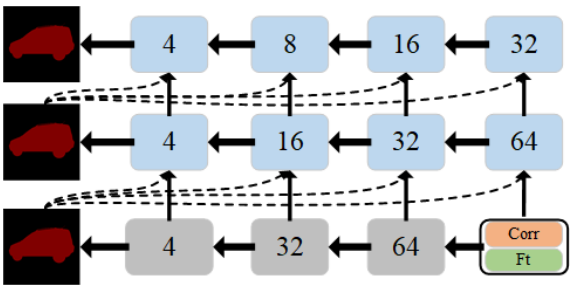

Figure 3. Illustration of the multi-resolution multi-stage segmentation network (MMS). We multiply the output of the last stage to features of the current stage (dashed lines) to filter background clutter and distracters. Horizontal: MRP, Vertical: MSP.

3.2. Multi-resolution Multi-stage Segmentation

The segmentation network is in charge of predicting a binary mask of the target. It contains a horizontal multi-resolution pathway and a vertical multi-stage pathway, as shown in Fig. 3. The multi-resolution pathway uses the features from different depths of the backbone network to progressively refine the feature maps. The multi-stage pathway utilizes the predicted mask from the last stage to filter the background clutter in features. The filtered features then go through another round of the multi-resolution pathway.

Multi-resolution pathway (MRP) combines the different information channels of the backbone network and progressively upscale the feature maps into an accurate and detailed segmentation mask. The first stage of MRP takes the enhanced backbone features $\hat{\mathbf{F}}_\mathbf{t}$ and the correlation feature form the Siamese tracking model (detailed in Sec. 4) as input. We fuse the correlation feature and $\hat{\mathbf{F}}_\mathbf{t}$ by element-wise addition. The correlation feature contains more target-correlated information, helping the segmentation network distinguish the target object from distractors. Then at each depth, the backbone features are first processed by a 3×3 convolutional layer followed by ReLU, and then fused with the output of last depth by point-wise addition,

$$O_d = conv(\mathcal{U}(O_{d+1})) + RELU(conv(b_d)) \tag{4}$$

where O_d and O_{d+1} denote output from depth d and $d+1$, respectively, *conv* indicates a 3×3 convolution layer and $\mathcal{U}$ is up-sampling operation, as represented by the green block in Fig. 4.

Multi-stage pathway (MSP) tends to filter the background clutter in the backbone features. We multiply the predicted mask from the last stage to backbone features in the current stage first, and then go through another round of MRP. To save computation cost, the number of channels is decreased at each depth to half of the last stage (except the layer before output), as shown in Fig. 3. The MSP only introduces small overhead to the segmentation network.

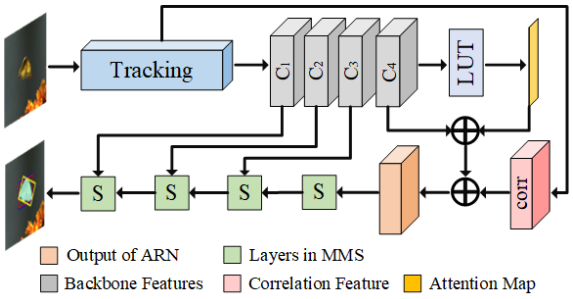

Figure 4. A simplified illustration of our *tracking-retrieval-segmentation* framework. The tracking model [50] outputs the backbone features ($c_1 - c_4$) and the correlation feature ("corr"). The attention retrieval network enhances the backbone feature c_4 and take it as the input of the MMS segmentation network. We only visualize the first stage of MMS here for conciseness.

3.3. Cyclic Initialization

Although we mainly focus on videos initialized with the mask in the starting frame, obtaining an accurate mask in the practical scenarios may be costly. This is also one of the barriers for propagation-based VOS methods to apply in practical products, since most videos are solely started with a bounding box. To improve our model's generality, we propose a cyclic initialization strategy to handle this issue.

We first generate a pseudo mask for the starting frame, where the pixels inside and outside the ground-truth box are set to 1 and 0, respectively. The pseudo mask is used to initialize the *values* of LUT. After that, we pass the starting frame through the model and predict a mask. The predicted mask is then used to re-initialize the *values* of LUT, and the starting frame is again passed through the model to get a new mask. We cyclically perform the re-initialization process for r times, and the mask used to initialize the LUT gradually becomes close to the real label. The cyclic initialization is easy to implement and guarantees that our model works well for both mask and bounding box initialization.

3.4. Relations to other Attention Mechanisms

Typical spatial and channel attention mechanisms [17, 42] learn weight map from a feature itself, lacking the theoretical interpretability of *how* it works. In the proposed attention retrieval network, we set a clear rule for *how* to learn, *i.e.* the pixels belonging to the target should be enhanced, and the pixels similar to background clutter should be weakened. The rule is guaranteed by learning the affinity between features of the testing frame and *addresses* in LUT. Notably, the attention map is related to both a feature itself and its references (*addresses* in LUT). This schema infuses the information of the starting frame and its label to the testing frame, which is not exploted in other proposed spatial attention mechanisms to our knowledge.

4. Framework

In this section, we describe the complete framework, as illustrated in Fig. 4.

Tracking. The object tracking follows the model structure and inference procedure in the recent proposed anchor-free Siamese approach Ocean [50]. It predicts a bounding box for the target, deciding the searching area in the next frame. The features from the *conv1-conv4* layers of the backbone network are extracted for the following segmentation task. The correlation feature from the feature combination module in Ocean is also preserved for the subsequent task (as detailed in Sec. 3.2). We refer the readers to Ocean [50] for more details about the tracking model.

Retrieval and Segmentation. The attention retrieval network uses the *conv4* feature of the staring frame and its corresponding mask to build the LUT. It first generates an attention map and then add the attention map to the *conv4* feature of the testing frame. Then, we add the enhanced *conv4* feature to the correlation feature from the tracking model. The output from the addition serves as the input of the first stage in the multi-resolution multi-stage network, as shown in Fig. 3. The MMS network progressively refines the feature map to output mask, as detailed in Sec. 3.2. The output channel in each resolution of the MMS is presented in Fig. 3.

Loss. To optimize the proposed framework, we consider both the content and contour of the mask in training.

$$\mathcal{L} = \mathcal{L}_{BCE}(y_p, y^*) + \lambda \mathcal{L}_{BCE}(y_p \times y_b^*, y_b^*) \qquad (5)$$

where $\mathcal{L}_{BCE}$ indicates the standard binary cross-entropy loss, y_p is the predicted mask and y^* is the mask label. y_b^* in Eq. 5 denotes the contour of the target in y^*. Concretely, we apply the official contour detection algorithm in OpenCV [4] on $y*$ to get y_b^*.

5. Experiments

5.1. Training

We train our framework with YouTube-VOS [44] and COCO [25]. The experiment is conducted on 8 GTX-2080Ti GPUs, with each GPU hosting 32 images. The training contains 50 epochs in total, taking about 8/12 hours for models wo/w MSP, respectively. Each epoch uses 2×10^5 training pairs. For the first 10 epochs, we use a warm-up learning rate exponentially increased from 10^{-3} to 10^{-2}. For the remaining epochs, the learning rate exponentially decayed from 10^{-2} to 5×10^{-3}. The weight decay and momentum are set to 10^{-3} and 0.9, respectively. The weight parameter λ in Eq. 5 is set to 0.1.

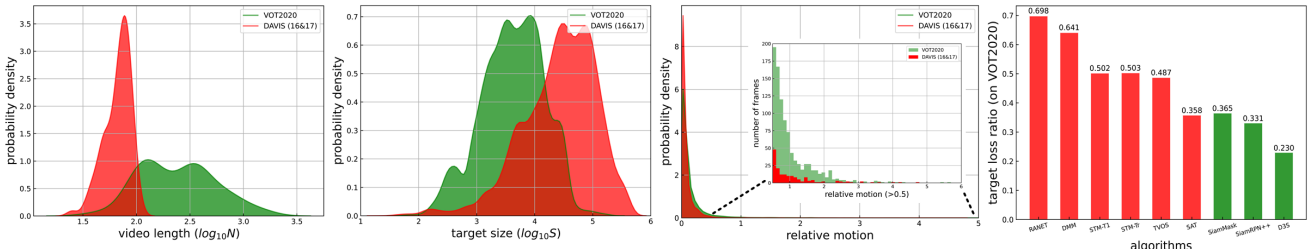

(a) (b) (c) (d)

Figure 5. $a - c$: comparison of data distribution in VOT2020 and DAVIS16&17 benchmarks, *i.e.,* video length, target size and relative motion. d : comparison of lost target ratio between VOS and VOT methods.

5.2. Evaluation

5.2.1 Benchmarks and Metrics

VOT. We evaluate our approach on recent proposed pixel-wise tracking benchmark, *i.e.,* VOT2020 [21]. It contains 60 video sequences, with an average length of 330 frames. We adopt the Expected Average Overlap (EAO) which takes both accuracy (A) and robustness (R) into account to evaluate overall performance.

VOS. We also evaluate our model under the semi-supervised protocol of widely used VOS benchmarks, *i.e.,* DAVIS16&17 [32]. The Jaccard index $\mathcal{J}$ and F-measure $\mathcal{F}$ are used to rank the models. The Jaccard index $\mathcal{J}$ describes the region similarity, and the F-measure $\mathcal{F}$ indicates contour accuracy of the predictions. For each measure, three statistics are considered: mean, recall, and decay, *e.g.* $\mathcal{F}_{\mathcal{M}}$, $\mathcal{F}_{\mathcal{O}}$ and $\mathcal{F}_{\mathcal{D}}$. The three indicators present the gain/loss of performance over time.

5.2.2 Compared Methods

We compare our model with state-of-the-art tracking methods, including SiamMASK [39], SiamRPN++ [23], SiamMargin [22], SiamFCOT [45], D3S [26], ATOM [11] and DiMP [3]. Among them, SiamMASK [39] and D3S [26] are capable of predicting segmentation mask. For other trackers, we employ an off-the-shelf algorithm, *i.e.,* Box2Seg [6], on them to satisfy the evaluation protocal of VOT2020. Moreover, we also evaluate algrithoms designed for video object segmentation, *i.e.*, OnAVOS [36], OSVOS [5], MSK [31], SFL [10], FAVOS [9], RGMP [43], PML [8], OSMN [46], PLM [34], VPN [20], CINN [1], VideoMatch [18], VM [18], STM [29], TVOS [48]. The results are presented in Tab. 1, Tab. 2 and Tab. 3.

5.2.3 Evaluation and Analysis on VOT

Tab. 1 shows the evaluation results on VOT2020. The comparisons and observations are summarized below.

Results Comparision 1) Although the official VOT2020 toolkit provides *bbox* evaluation mode, simply conducting a segmentation method after tracking can significantly improve the performance. For example, when equipping SiamRPN++ [23] with Box2Seg [6], the accuracy achieves gains of 15.4 points. 2) The proposed offline and online models achieve the best performance (EAO) among all compared trackers. We observed that the proposed offline model surpasses SiamMASK [39] for more than 11 points with small computation overhead, demonstrating the potentiality of our approach. Comparing our offline version with the online tracker D3S [26], it shows that the gains

Output	Method	M	EAO ↑	Acc.↑	Rob.↑	FPS↑
bbox	SiamRPN++ [23]	✗	0.247	0.435	0.670	–
	SiamR-CNN [37]	✗	0.233	0.458	0.610	–
	SiamMargin[22]	✗	0.226	0.415	0.637	–
	SiamFCOT [45]	✗	0.247	0.421	0.703	–
	ATOM [11]	✗	0.268	0.437	0.715	–
	DiMP [3]	✗	0.281	0.448	0.743	–
mask(vos)	SAT [7]	✓	0.363	0.641	0.642	29
	FRTM [33]	✓	0.211	0.437	0.510	30
	RANET [41]	✓	0.108	0.226	0.302	8
	DMM [47]	✓	0.172	0.409	0.359	12
	STM-T1 [29]	✓	0.292	0.620	0.498	4
	STM-Tr [29]	✓	0.294	0.675	0.496	15
	TVOS [48]	✓	0.303	0.621	0.513	40
mask (vot)	SiamMask [39]	✗	0.328	0.589	0.634	55
	D3S [26]	✗	0.414	0.613	0.770	25
	SiamRPN++/Box2Seg [6]	✗	0.379	0.675	0.646	18
	SiamR-CNN/Box2Seg [6]	✗	0.355	0.699	0.586	4
	SiamMargin/Box2Seg [6]	✗	0.349	0.669	0.603	17
	SiamFCOT/Box2Seg [6]	✗	0.409	0.674	0.695	27
	ATOM/Box2Seg [6]	✗	0.382	0.659	0.663	15
	DiMP/Box2Seg [6]	✗	0.406	0.672	0.691	17
	Ours (offline)	✓	0.444	0.648	0.754	40
	Ours (online)	✓	0.500	0.648	0.842	20

Table 1. Quantitative results on the VOT2020. "Output" indicates the prediction format. "M" denotes use the mask in the starting frame. "EAO", "Acc." and "Rob." are expected overlap ratio, accuracy and robustness, respectively. "FPS" indicates running speeds, *i.e.,* frame-per-second.

come from mask *accuracy*, indicating the effectiveness of our segmentation network under challenging tracking scenarios. When equipped with the online branch [50], we obtain further performance improvement, *i.e.,* EAO of 0.5.

Why VOS Methods Perform Poorly We observed that the top-ranked VOS methods, *e.g.* STM [29], TVOS [48], perform even worse than the baseline tracker SiamMask [39]. We argue that the underlying reason lies in data distribution, as depicted in Fig. 5. VOS task typically considers large targets observed for less than 100 frames with low background distractor presence (Fig. 5 (a)(b)). While in object tracking benchmarks, the videos are usually longer (Fig. 5 (a)), the size of targets is relatively small (Fig. 5 (b)), and the motion (compared to the target's size) is relatively large (Fig. 5 (c)). The VOS approaches thus fare poorly in challenging tracking scenarios (Fig. 5 (d)). Besides, we experimentally observed that propagation-based methods like [48] and [29] suffer from memory constraints since they usually store the intermediate features and masks of each frame. When the sequence goes longer (*e.g.* $\geq$ 300 frames), memory error may appear.

5.2.4 Evaluation and Analysis on VOS

The results of DAVIS16&17 are presented in Tab. 2 and Tab. 3, respectively. We only use the offline tracker when testing on VOS benchmarks unless otherwise specified, since the target in VOS videos is easy to track.

Results Comparision Compared to SiamMask [39], which is also conducted on a Siamese tracker, our approach obtains gains of 3.6 / 5.4 points on $\mathcal{J}\&\mathcal{F}$ for DAVIS16/17, respectively. Notably, we achieve better performances than SiamMask [39] and D3S [26] on all seven criteria of DAVIS17, demonstrating the effectiveness of our approach. Moreover, both our approach and SiamMask [39] can run in per-frame real-time speeds, which are much faster than most VOS methods (see Fig. 1). This guarantees that our method can serve as a strong baseline for VOS.

Why VOT Methods are Generally Lagging An observation is that top-ranked VOS methods generally surpass the VOT approaches. The underlying reason is that VOT methods typically consider both robustness tracking and accurate segmentation. To ensure the fast inference speed, the mask branch's weight parameters often take only a fraction of the whole network, *e.g.,* $\leq 5\%$ in our model. Most VOS methods, *e.g.* STM [29] and TVOS [48] perform segmentation without considering tracking. Thus, one potential research direction is designing a model that conquers both VOT and VOS tasks while keeping fast inference speed.

5.3. Further Analysis

Cyclic Initialization. To increase the generality of our model, *i.e.* tracking on videos without mask initialization,

	$\mathcal{J}\&\mathcal{F}_{\uparrow}$	$\mathcal{J}_{\mathcal{M}\uparrow}$	$\mathcal{J}_{\mathcal{O}\uparrow}$	$\mathcal{J}_{\mathcal{D}\downarrow}$	$\mathcal{F}_{\mathcal{M}\uparrow}$	$\mathcal{F}_{\mathcal{O}\uparrow}$	$\mathcal{F}_{\mathcal{D}\downarrow}$	FPS
OnAVOS[36]	85.5	86.1	96.1	5.2	84.9	89.7	5.8	0.1
RGMP[43]	81.8	81.5	91.7	10.9	82.0	90.8	10.1	8
FAVOS[9]	81.0	82.4	96.5	4.5	79.5	89.4	5.5	0.8
OSVOS[5]	80.2	79.8	93.6	14.9	80.6	92.6	15.0	0.1
MSK[31]	77.6	79.7	93.1	8.9	75.4	87.1	9.0	0.1
PML[8]	77.4	75.5	89.6	8.5	79.3	93.4	7.8	3.6
SFL[10]	76.1	76.1	90.6	12.1	76.0	85.5	10.4	0.1
OSMN[46]	73.5	74.0	87.6	9.0	72.9	84.0	10.6	8.0
VPN[20]	67.9	70.2	82.3	12.4	65.5	69.0	14.4	1.6
PLM[34]	66.4	70.2	86.3	11.2	62.5	73.2	14.4	6.7
D3S[26]	74.0	75.4	-	-	72.6	-	-	25
SiamMASK[39]	69.8	71.7	86.8	3.0	67.8	79.8	2.1	58
Ours	73.4	74.7	91.1	5.0	72.1	85.9	5.3	40

Table 2. Results on DAVIS2016 validation set. Our model surpasses SiamMask [39] with sizable margin and achieves comparable performance with D3S [26] while running in 2$\times$ faster.

	$\mathcal{J}\&\mathcal{F}_{\uparrow}$	$\mathcal{J}_{\mathcal{M}\uparrow}$	$\mathcal{J}_{\mathcal{O}\uparrow}$	$\mathcal{J}_{\mathcal{D}\downarrow}$	$\mathcal{F}_{\mathcal{M}\uparrow}$	$\mathcal{F}_{\mathcal{O}\uparrow}$	$\mathcal{F}_{\mathcal{D}\downarrow}$	FPS
TVOS[48]	72.3	69.9	-	-	74.7	-	-	39
STM[29]	71.6	69.2	-	-	74.0	-	-	15
RGMP [43]	66.7	64.8	-	-	68.6	-	-	8
VM[18]	62.4	68.2	-	-	54.6	-	-	3
OSVOS[5]	60.3	56.6	63.8	26.1	63.9	73.8	27.0	0.1
FAVOS [9]	58.2	54.6	-	-	61.8	-	-	0.8
OSMN[46]	54.8	52.5	60.9	21.5	57.1	66.1	24.3	8.0
D3S[26]	60.8	57.8	-	-	63.8	-	-	25
SiamMASK[39]	56.4	54.3	62.8	19.3	58.5	67.5	20.9	55
Ours	61.9	58.9	68.7	18.2	64.9	76.9	18.5	40

Table 3. Results on DAVIS2017 validation set. We achieve better results than SiamMask [39] and D3S [26] on all seven criteria, demonstrating the effectiveness of our approach.

we impose a cyclic initialization strategy during inference. We visualize the predicted mask at each cyclic step in Fig. 6. The mask's quality of the starting frame (*values* in LUT) is improved with the increasing of cyclic steps (see Fig. 6 (a)). We set the cyclic steps r to 3 unless otherwise specified. Fig. 6 (b) presents the results in the subsequent frames after cyclic initialization, achieving promising results. Besides, there is an alternative initiation strategy, *i.e.,* estimating mask with Box2Seg [6] in the starting frame. Although also effective, it is not as flexible and fast as the cyclic initialization strategy.

False-Positive Analysis. We conduct an ablation experiment to verify the effectiveness of our model on reducing false-positive predictions. Correctly, we define an evaluation criterion, namely the false-positive ratio (FPR),

$$FPR = \frac{1}{N}\sum\nolimits_{i} FP/s \tag{6}$$

where N is the number of frames, FP indicates the number of false-positive pixels in a frame, and s is the size of the target. We consider the target's size in experiments in case it introduces unfair comparison, *i.e.,* large objects may bring

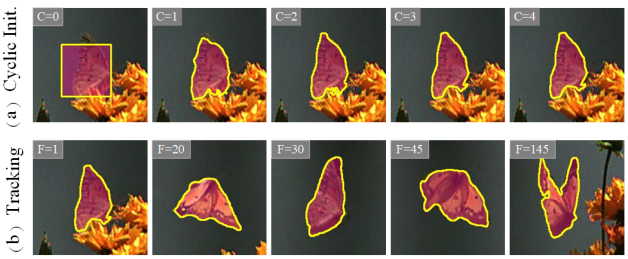

Figure 6. Visualization of the predicted mask in each step of cyclic initialization (a) and the tracking results based on cyclic initialization (b). It shows that the estimated mask becomes better with the increasing of cyclic steps. The cyclic initialization is thus capable of building a reasonable LUT for the subsequent tracking.

more false-positive pixels than small ones. The comparison results are presented in Tab. 4. Without the multi-stage pathway (MSP), our FPR is 19.1%, much lower than 28.2% of D3S [26] and 42.1% of SiamMask [39]. When equipped with MSP, the FPR of our model decreases to 17.0%. The experiments demonstrate the superiority of the proposed attention retrieval network (ARN) and multi-stage pathway (MSP) on reducing false-positive predictions.

w/wo Attention Retrieval Network (ARN). To verify the efficacy of the proposed attention retrieval network (ARN), we perform ablation experiments on VOT2020 [21], as shown in Tab. 5. Without ARN, the baseline method obtains an EAO of 0.387 and an accuracy of 0.623. We evaluate three variants of ARN, *i.e.* concatenation (con.), multiplication(mul.), and addition (add.), indicating how we apply the learned attention map to backbone features. It shows that the addition format performs better, outperforming the baseline model with 5.6 points on EAO and 2.3 points on accuracy. We observed that the addition format surpasses the multiplication. One possible reason is that directly filter out all background pixels in the starting of segmentation may inevitably hurt the boundary learning in the segmentation phase.

Stages in Multi-Stage Pathway (MSP). In SiamMask [39] and D3S [26], a multi-resolution segmentation pathway is arranged to progressively refine the feature map to accurate mask. In our work, we further introduce a multi-stage pathway (MSP) to reuse the predicted mask to filter background pixels in backbone features. As shown in Tab. 6, we achieve the best performance, *i.e.,* $\mathcal{J}\&\mathcal{F}$ of 0.734 on DAVIS16 and accuracy of 0.656 on VOT2020, when the number of stages is 3. When removing the MSP, the $\mathcal{J}\&\mathcal{F}$ and accuracy degrade to 0.705 (-2.9 points) and 0.647 (-0.8 points), respectively. Notably, the channels are truly light in the additional introduced stages, introducing small computation overhead.

	SiamMask [39]	D3S [26]	Ours	Ours-M
FPR (%) ↓	42.1	28.2	19.1	17.0

Table 4. Ablation experiments on false-positive ratio. "Ours" and "Ours-M" indicate w/wo multi-stages pathway(MSP).

	without	con.	mul.	add.
Acc. ↑	0.623	0.630	0.638	0.647
EAO ↑	0.388	0.412	0.433	0.444

Table 5. Ablation experiments on ARN. "con.", "mul." and "add." indicate concatenation, multiplication and addition when we apply the attention to backbone features.

	1	2	3	4
Acc. ↑	0.647	0.651	0.656	0.652
$J\&F$ ↑	0.705	0.721	0.734	0.723

Table 6. Ablation experiments on multi-stage pathway (MSP). We present the results of $\mathcal{J}\&\mathcal{F}$ on DAVIS16 and segmentation accuracy in VOT2020.

Upper-bound Analysis. We design an experiment to analyze the upper bound of the proposed segmentation network. To alleviate the influence of the tracking network, we provide the ground-truth, *i.e.,* target location and scale of each frame, to the model. We then evaluate the segmentation accuracy, *i.e. mIoU* (mean intersection over union), on VOT2020. Without considering tracking, our segmentation network achieves *mIoU* of 0.71, leaving an improvement room of 6.3 points compared to 0.647 in Tab. 5. We also study replacing the multi-resolution pathway (MRP) to a complex structure, *i.e.,* UNet++ [51], and obtain *mIoU* of 0.76, which further improves the ceiling of our model. In future work, we will study how to unleash the complex model's capability while keeping efficiency.

6. Conclusion

In this work, we introduce the attention retrieval network (ARN) to mitigate the false positive predictions in the paradigm of tracking with a segmentation side-branch. The attention retrieval network learns an attention map to set soft spatial constraints on the backbone features, by which the negative influence of backbone clutter are weakened. We then further propose the multi-stage pathway on the typical multi-resolution segmentation network. The mask predicted from the last stage helps filter the background pixels in features of the current stage. We also impose the cyclic initialization to apply our framework on videos without mask initialization. The experiments demonstrate the effectiveness and efficiency of our approach on both VOT and VOS benchmarks.

References

[1] Linchao Bao, Baoyuan Wu, and Wei Liu. Cnn in mrf: Video object segmentation via inference in a cnn-based higher-order spatio-temporal mrf. In *CVPR*, pages 5977–5986, 2018. 6

[2] Luca Bertinetto, Jack Valmadre, Joao F Henriques, Andrea Vedaldi, and Philip HS Torr. Fully-convolutional siamese networks for object tracking. In *ECCV Workshop*, pages 850–865. Springer, 2016. 2

[3] Goutam Bhat, Martin Danelljan, Luc Van Gool, and Radu Timofte. Learning discriminative model prediction for tracking. In *ICCV*, pages 6182–6291, 2019. 6

[4] G. Bradski. The OpenCV Library. *Dr. Dobb's Journal of Software Tools*, 2000. 5

[5] Sergi Caelles, Kevis-Kokitsi Maninis, Jordi Pont-Tuset, Laura Leal-Taixé, Daniel Cremers, and Luc Van Gool. One-shot video object segmentation. In *CVPR*, pages 221–230, 2017. 3, 6, 7

[6] Liang-Chieh Chen, Yukun Zhu, George Papandreou, Florian Schroff, and Hartwig Adam. Encoder-decoder with atrous separable convolution for semantic image segmentation. In *ECCV*, pages 801–818, 2018. 1, 6, 7

[7] Xi Chen, Zuoxin Li, Ye Yuan, Gang Yu, Jianxin Shen, and Donglian Qi. State-aware tracker for real-time video object segmentation. In *CVPR*, pages 9384–9393, 2020. 6

[8] Yuhua Chen, Jordi Pont-Tuset, Alberto Montes, and Luc Van Gool. Blazingly fast video object segmentation with pixel-wise metric learning. In *CVPR*, pages 1189–1198, 2018. 6, 7

[9] Jingchun Cheng, Yi-Hsuan Tsai, Wei-Chih Hung, Shengjin Wang, and Ming-Hsuan Yang. Fast and accurate online video object segmentation via tracking parts. In *CVPR*, pages 7415–7424, 2018. 6, 7

[10] Jingchun Cheng, Yi-Hsuan Tsai, Shengjin Wang, and Ming-Hsuan Yang. Segflow: Joint learning for video object segmentation and optical flow. In *ICCV*, pages 686–695, 2017. 6, 7

[11] Martin Danelljan, Goutam Bhat, Fahad Shahbaz Khan, and Michael Felsberg. Atom: Accurate tracking by overlap maximization. In *CVPR*, pages 4660–4669, 2019. 2, 6

[12] Martin Danelljan, Goutam Bhat, Fahad Shahbaz Khan, Michael Felsberg, et al. Eco: Efficient convolution operators for tracking. In *CVPR*, pages 6931–6939, 2017. 2

[13] Qi Fan, Wei Zhuo, Chi-Keung Tang, and Yu-Wing Tai. Few-shot object detection with attention-rpn and multi-relation detector. In *CVPR*, pages 4013–4022, 2020. 3

[14] Jun Fu, Jing Liu, Haijie Tian, Yong Li, Yongjun Bao, Zhiwei Fang, and Hanqing Lu. Dual attention network for scene segmentation. In *CVPR*, pages 3146–3154, 2019. 3

[15] Kaiming He, Georgia Gkioxari, Piotr Dollár, and Ross Girshick. Mask r-cnn. In *Proceedings of the IEEE international conference on computer vision*, pages 2961–2969, 2017. 1

[16] João F Henriques, Rui Caseiro, Pedro Martins, and Jorge Batista. High-speed tracking with kernelized correlation filters. *TPAMI*, 37(3):583–596, 2014. 2

[17] Jie Hu, Li Shen, and Gang Sun. Squeeze-and-excitation networks. In *CVPR*, pages 7132–7141, 2018. 3, 5

[18] Yuan-Ting Hu, Jia-Bin Huang, and Alexander G Schwing. Videomatch: Matching based video object segmentation. In *ECCV*, pages 54–70, 2018. 3, 6, 7

[19] Laurent Itti, Christof Koch, and Ernst Niebur. A model of saliency-based visual attention for rapid scene analysis. *TPAMI*, pages 1254–1259, 1998. 3

[20] Varun Jampani, Raghudeep Gadde, and Peter V Gehler. Video propagation networks. In *CVPR*, pages 451–461, 2017. 6, 7

[21] Matej Kristan, Jiri Matas, Ales Leonardis, and Felsberg. The eighth visual object tracking vot2020 challenge results. In *ECCV Workshops*, pages 0–0, 2020. 1, 2, 6, 8

[22] Matej Kristan, Jiri Matas, Ales Leonardis, Michael Felsberg, and Roman Pflugfelder. The seventh visual object tracking vot2019 challenge results. In *ICCV Workshops*, pages 0–0, 2019. 6

[23] Bo Li, Wei Wu, Qiang Wang, Fangyi Zhang, Junliang Xing, and Junjie Yan. Siamrpn++: Evolution of siamese visual tracking with very deep networks. In *CVPR*, pages 4282–4291, 2019. 2, 6

[24] Bo Li, Junjie Yan, Wei Wu, Zheng Zhu, and Xiaolin Hu. High performance visual tracking with siamese region proposal network. In *CVPR*, pages 8971–8980, 2018. 2

[25] Tsung-Yi Lin, Michael Maire, Serge Belongie, James Hays, Pietro Perona, Deva Ramanan, Piotr Dollár, and C Lawrence Zitnick. Microsoft coco: Common objects in context. In *ECCV*, pages 740–755, 2014. 5

[26] Alan Lukezic, Jiri Matas, and Matej Kristan. D3s-a discriminative single shot segmentation tracker. In *CVPR*, pages 7133–7142, 2020. 1, 2, 6, 7, 8

[27] K-K Maninis, Sergi Caelles, Yuhua Chen, Jordi Pont-Tuset, Laura Leal-Taixé, Daniel Cremers, and Luc Van Gool. Video object segmentation without temporal information. *TPAMI*, 41(6):1515–1530, 2018. 3

[28] Seyed Mojtaba Marvasti-Zadeh, Li Cheng, Hossein Ghanei-Yakhdan, and Shohreh Kasaei. Deep learning for visual tracking: A comprehensive survey. *arXiv preprint arXiv:1912.00535*, 2019. 2

[29] Seoung Wug Oh, Joon-Young Lee, Ning Xu, and Seon Joo Kim. Video object segmentation using space-time memory networks. In *ICCV*, pages 9226–9235, 2019. 3, 6, 7

[30] Federico Perazzi, Anna Khoreva, Rodrigo Benenson, Bernt Schiele, and Alexander Sorkine-Hornung. Learning video object segmentation from static images. In *CVPR*, pages 2663–2672, 2017. 3

[31] Federico Perazzi, Anna Khoreva, Rodrigo Benenson, Bernt Schiele, and Alexander Sorkine-Hornung. Learning video object segmentation from static images. In *CVPR*, pages 2663–2672, 2017. 6, 7

[32] Federico Perazzi, Jordi Pont-Tuset, Brian McWilliams, Luc Van Gool, Markus Gross, and Alexander Sorkine-Hornung. A benchmark dataset and evaluation methodology for video object segmentation. In *CVPR*, pages 724–732, 2016. 6

[33] Andreas Robinson, Felix Jaremo Lawin, Martin Danelljan, Fahad Shahbaz Khan, and Michael Felsberg. Learning fast and robust target models for video object segmentation. In *CVPR*, pages 7406–7415, 2020. 6

[34] Jae Shin Yoon, Francois Rameau, Junsik Kim, Seokju Lee, Seunghak Shin, and In So Kweon. Pixel-level matching for video object segmentation using convolutional neural networks. In *ICCV*, pages 2167–2176, 2017. 6, 7

[35] Paul Voigtlaender, Yuning Chai, Florian Schroff, Hartwig Adam, Bastian Leibe, and Liang-Chieh Chen. Feelvos: Fast end-to-end embedding learning for video object segmentation. In *CVPR*, pages 9481–9490, 2019. 3

[36] Paul Voigtlaender and Bastian Leibe. Online adaptation of convolutional neural networks for video object segmentation. In *BMVC*, pages 1000–1008, 2017. 6, 7

[37] Paul Voigtlaender, Jonathon Luiten, Philip HS Torr, and Bastian Leibe. Siam r-cnn: Visual tracking by re-detection. In *CVPR*, pages 6578–6588, 2020. 1, 2, 3, 6

[38] Qiang Wang, Zhu Teng, Junliang Xing, Jin Gao, Weiming Hu, and Stephen Maybank. Learning attentions: residual attentional siamese network for high performance online visual tracking. In *CVPR*, pages 4854–4863, 2018. 3

[39] Qiang Wang, Li Zhang, Luca Bertinetto, Weiming Hu, and Philip HS Torr. Fast online object tracking and segmentation: A unifying approach. In *CVPR*, pages 1328–1338, 2019. 1, 2, 6, 7, 8

[40] Xudong Wang, Zhaowei Cai, Dashan Gao, and Nuno Vasconcelos. Towards universal object detection by domain attention. In *CVPR*, pages 7289–7298, 2019. 3

[41] Ziqin Wang, Jun Xu, Li Liu, Fan Zhu, and Ling Shao. Ranet: Ranking attention network for fast video object segmentation. In *ICCV*, pages 3978–3987, 2019. 6

[42] Sanghyun Woo, Jongchan Park, Joon-Young Lee, and In So Kweon. Cbam: Convolutional block attention module. In *ECCV*, pages 3–19, 2018. 5

[43] Seoung Wug Oh, Joon-Young Lee, Kalyan Sunkavalli, and Seon Joo Kim. Fast video object segmentation by reference-guided mask propagation. In *CVPR*, pages 7376–7385, 2018. 6, 7

[44] Ning Xu, Linjie Yang, Yuchen Fan, Dingcheng Yue, Yuchen Liang, Jianchao Yang, and Thomas Huang. Youtube-vos: A large-scale video object segmentation benchmark. *arXiv preprint arXiv:1809.03327*, 2018. 5

[45] Yinda Xu, Zeyu Wang, Zuoxin Li, Ye Yuan, and Gang Yu. Siamfc++: Towards robust and accurate visual tracking with target estimation guidelines. In *AAAI*, pages 12549–12556, 2020. 2, 6

[46] Linjie Yang, Yanran Wang, Xuehan Xiong, Jianchao Yang, and Aggelos K Katsaggelos. Efficient video object segmentation via network modulation. In *CVPR*, pages 6499–6507, 2018. 6, 7

[47] Xiaohui Zeng, Renjie Liao, Li Gu, Yuwen Xiong, Sanja Fidler, and Raquel Urtasun. Dmm-net: Differentiable mask-matching network for video object segmentation. In *ICCV*, pages 3929–3938, 2019. 6

[48] Yizhuo Zhang, Zhirong Wu, Houwen Peng, and Stephen Lin. A transductive approach for video object segmentation. In *CVPR*, June 2020. 3, 6, 7

[49] Zhipeng Zhang and Houwen Peng. Deeper and wider siamese networks for real-time visual tracking. In *CVPR*, pages 4591–4600, 2019. 2

[50] Zhipeng Zhang, Houwen Peng, Jianlong Fu, Bing Li, and Weiming Hu. Ocean: Object-aware anchor-free tracking. In *ECCV*, 2020. 2, 3, 5, 7

[51] Zongwei Zhou, Md Mahfuzur Rahman Siddiquee, Nima Tajbakhsh, and Jianming Liang. Unet++: A nested u-net architecture for medical image segmentation. In *DLMIAML-CDS*, pages 3–11. Springer, 2018. 8